

FDTD solutions for the distribution of radiation from dipoles embedded in dielectric particles

Changhui Li^{a,*}, George W. Kattawar^a, Yu You^a, Pengwang Zhai^a, Ping Yang^b

^a*Department of Physics, Texas A&M University, College Station, TX, USA*

^b*Department of Atmospheric Sciences, Texas A&M University, College Station, TX, USA*

Abstract

The finite-difference time-domain (FDTD) method is used to simulate the electromagnetic radiation emitted by an infinitesimal electric dipole embedded in a small particle with an arbitrary shape and internal composition. The far-field pattern of the radiation pertaining to dipoles embedded in a host particle is highly sensitive to the particle shape. Thus, it is possible to discriminate host particles according to their radiation patterns. The method reported here is also applicable to the study of induced Raman scattering and fluorescence phenomena and the detection of biological agents.

© 2007 Published by Elsevier Ltd.

Keywords: Finite-difference time-domain method; Electric dipole radiation; Non-spherical particle

1. Introduction

Raman scattering and fluorescence effects are of great interest to many disciplines including remote sensing [1], biological agent detection [2], and cell structure identification. Both Raman scattering and fluorescence processes are quantum-state transitions at molecular level, which, however, are widely assumed as electric dipole transitions. The sizes of particles that contain the molecules triggering Raman scattering or fluorescence radiation are usually comparable with the wavelength of the radiated field. Thus, the applicability of geometric optics breaks down in this case. The analytical solutions for the radiation emitted by an electric dipole embedded within a small host particle with spherical or ellipsoidal geometry have been reported in the literatures [3–5]. It is shown that both the total radiation power and the spatial distribution of radiated energy depend on the position and orientation of the dipole and the refractive index of the host particle. Usually, the shapes of host particles exhibiting fluorescence and Raman scattering are irregular. Thus, it is important to understand the radiation field induced by infinitesimal electric dipoles embedded in small particles with arbitrary shapes and compositions. To our best knowledge, only a handful of studies have been carried out to numerically simulate the radiation by infinitesimal electric dipoles in small particles or cavities [6].

*Corresponding author.

E-mail address: cli@biomed.wustl.edu (C. Li).

2. Simulation method

In this study, we use the finite-difference time-domain (FDTD) [7,8] method to simulate the radiation pertaining to an infinitesimal dipole with an arbitrary orientation and position. A time function is needed to describe the dipole source before the simulation. For example, a Gaussian function is used in the time domain in the form of

$$\mathbf{p}(t) = \mathbf{p}_0 e^{-(t-T_0)^2/\sigma^2}, \quad (1)$$

where \mathbf{p}_0 is a constant vector representing the strength and orientation of the dipole, σ and T_0 are two parameters specifying, respectively, the width and center of the Gaussian pulse in the time domain. The dipole is assumed to be a “hard” source, that is, the strength of the dipole is independent of the ambient electric field. After several simple mathematical derivations [9], the electric field can be calculated in the form of

$$\mathbf{E}(\mathbf{r}, t) = \frac{1}{4\pi\epsilon} \nabla \times \left[\nabla \times \frac{\mathbf{p}(t - r/c)}{r} \right], \quad (2)$$

where ϵ is the medium permittivity.

Fig. 1 shows two typical FDTD grid cells with a grid resolution specified by the parameters Δx , Δy , and Δz . A spatial location in the discretized space is denoted by the indices $(I, J, K) = (I\Delta x, J\Delta y, K\Delta z)$. As the same as in the conventional FDTD algorithm, we define the electric and magnetic fields at the centers of the cell edges and the center of the cell faces, respectively. Note that electric fields E_x and E_y shown in Fig. 1 also represent the path-averaged (along the grid edges) values. Similarly, the magnetic fields represent the values averaged over the cell faces. Because the field values along the grid edges close to the dipole are quite sensitive to the distance and direction of the dipole, field values at the centers of these edges are not good approximations to represent the corresponding path-averaged values. Therefore, to simulate the radiation from infinitesimal electric dipole, as shown in Fig. 1, we modified the conventional FDTD by calculating the exact path-average field values from Eq. (2) on edges of a grid that contains the dipole.

As shown in Fig. 1, we apply the Faraday’s law to the shaded area in Fig. 1 so that we have

$$\int_l \mathbf{E} \cdot d\mathbf{l} = \frac{\partial}{\partial t} \int_s B_z ds, \quad (3)$$

where the path of the preceding integral is along the direction shown in Fig. 1. According to our modification, the path integral of the electric field values is replaced by the product of the field value at the center of the edge and the grid size except for the edge nearest to the dipole. The surface integral for the magnetic field is also replaced approximately by the product of the area of the cell face and the field value at the center of the cell

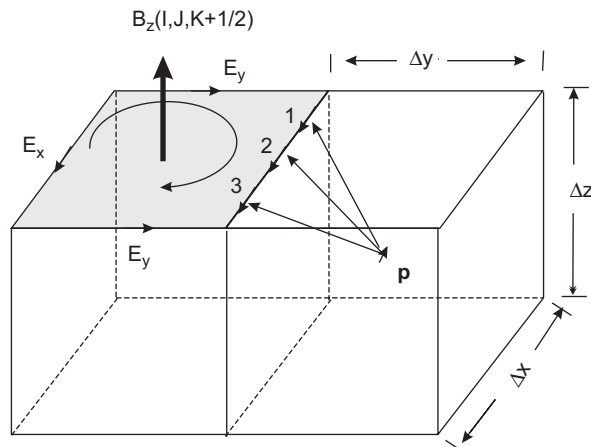


Fig. 1. Modification of FDTD in simulation of the dipole radiation.

face. Thus, the path integral operation is only applied to the edges of the grid that contains the dipole. After some mathematical manipulations, the numerical scheme for updating can be written as follows:

$$\frac{B_z^{n+1/2}(I, J, K + \frac{1}{2}) - B_z^{n-1/2}(I, J, K + \frac{1}{2})}{\Delta t} = \frac{1}{\Delta x} \left[E_y^n \left(I - \frac{1}{2}, J, K + \frac{1}{2} \right) - E_y^n \left(I + \frac{1}{2}, J, K + \frac{1}{2} \right) \right] + \frac{1}{\Delta y} \left[\int_I^{I+1} E_x^n \left(l, J + \frac{1}{2}, K + \frac{1}{2} \right) dl - E_x^n \left(I, J - \frac{1}{2}, K + \frac{1}{2} \right) \right], \quad (4)$$

where the superscripts represent the discretized temporal indices. Although the simulations are in the time domain, we can apply a Fourier transformation to both the dipole source and the simulated values in the time domain to obtain the dipole radiation in the frequency domain.

3. Simulation results

Fig. 2 shows the simulated angular distribution of the radiated field from a dipole within a sphere in comparison with the analytical counterpart. The sphere has a radius of $8.0 \mu\text{m}$ and the radiated field wavelength is $6.28 \mu\text{m}$. The refractive index of the sphere is 1.33. The dipole is located at $\frac{1}{2}$ of the radius along the radial direction. The results are normalized by the maximum value. Clearly, the present results are quite consistent with the analytical solutions in most of the angular region.

For the radiation from dipoles embedded in non-spherical shapes, we computed the far-field radiation pattern for a dipole inside a cube or a cylinder as shown in Fig. 3, where angular distribution of the radiation in azimuthal angle $\phi = 0$ plane are shown. Same wavelength and refractive index values are used as in Fig. 2 for both cases. The width of the cube is $12.90 \mu\text{m}$. The radius of the cylinder is $6.99 \mu\text{m}$ and the height of the cylinder is twice the radius. Both the cube and cylinder have the same volume as the sphere in Fig. 2. The infinitesimal dipoles are embedded at the centers of the particles with the directions along the z -axis. The value of the intensity is normalized by its maximum value as did in Fig. 2. We also compare our results with the discrete dipole approximation (DDA) [10] solutions. As shown in the figure, those patterns are quite different from those for sphere in that, for the latter, the maximum of the radiated field by the centered dipole is observed for a polar angle of $\theta = 90^\circ$. The far-field radiation pattern is highly sensitive to the particle shape. Thus, it is possible to discriminate host particles according to their radiation patterns.

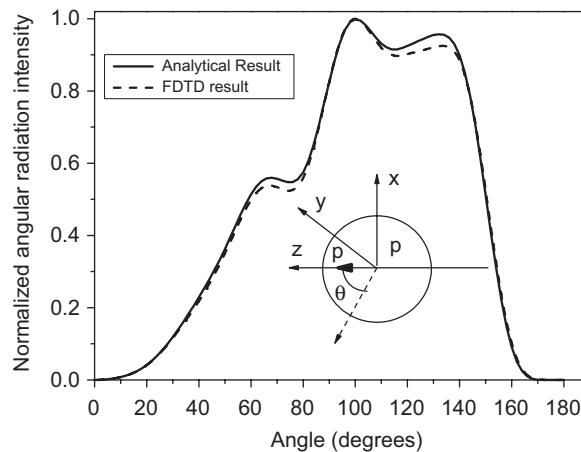


Fig. 2. Comparison of the angular distribution of the radiation field from a dipole in a spherical particle with radius $8.0 \mu\text{m}$, wavelength is $6.28 \mu\text{m}$, and the refractive index $m = 1.33$. The dipole is located at $\frac{1}{2}$ of the radius and oriented in the radial direction.

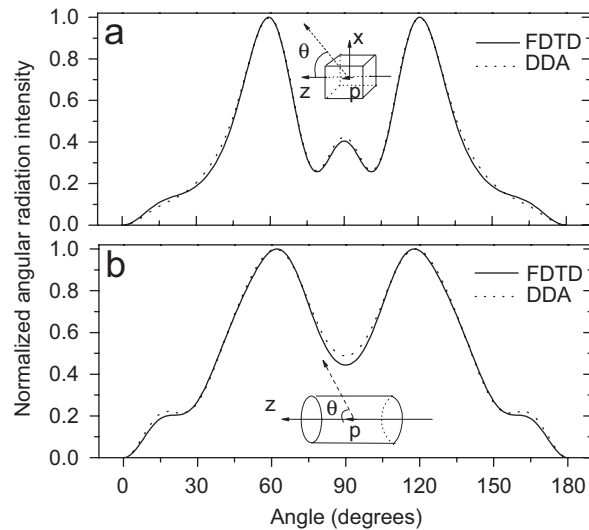


Fig. 3. Radiation from the dipole inside cube and cylinder which has a same volume and refractive index as the sphere in Fig. 2, in both cases, the direction of the dipole is along the z -axis: (a) normalized angular radiation intensity vs. polar angle for a centered dipole inside the homogenous cube; (b) normalized angular radiation intensity vs. polar angle for a centered dipole inside the homogenous cylinder.

4. Discussions

Although we only simulated the radiation field pertaining to a single dipole, it is straightforward to apply the present method to the case for multi-dipoles. Compared with the method used in [6], our method is based on a “real” infinitesimal electric dipole instead of a uniformly distributed dipole source in a grid. Compared with the DDA method, FDTD has some advantages such as the latter can be used for larger particles and it can simulate the radiation process in the time domain. Moreover, the FDTD method is more convenient for simulating surface enhanced cases where the particle is close to a metal surface. It is also possible to apply this method to study induced Raman scattering and fluorescence phenomena if the molecules embedded in host particles are known.

Acknowledgments

George Kattawar’s effort is supported by the Office of Naval Research under contracts N00014-02-1-0478 and N00014-06-1-0069. Ping Yang’s effort is supported by the National Science Foundation Physical Meteorology Program (ATM-0239605) managed by Dr. Andrew Detwiler and a research grant (NNG04GL24G) from NASA Radiation Sciences Program managed by Dr. Hal Maring (previously by Dr. Donald Anderson).

References

- [1] Immler F, Engelbart D, Schrems O. Fluorescence from atmospheric aerosol detected by a lidar indicates biogenic particles in the lowermost stratosphere. *Atmos Chem Phys* 2005;5:345–55.
- [2] Pinnick RG, Hill SC, Nachman P, Pendleton JD, Fernandez GL, Mayo MW, et al. Fluorescence particle counter for detecting airborne bacteria and other biological particles. *Aerosol Sci Technol* 1995;23:653–64.
- [3] Chew H, McNulty PJ, Kerker M. Model for Raman and fluorescent scattering by molecules embedded in small particles. *Phys Rev A* 1976;13:396–404.
- [4] Chew H. Transition rates of atoms near spherical surfaces. *J Chem Phys* 1987;87:1355–60.
- [5] Chew H. Radiation lifetime of atoms inside dielectric particles. *Phys Rev A* 1988;38:3410–6.
- [6] Xu Y, Vučković JS, Lee RK, Painter OJ, Scherer A, Yariv A. Finite-difference time-domain calculation of spontaneous emission lifetime in a microcavity. *J Opt Soc Am B* 1998;36:465–74.

- [7] Yee KS. Numerical solution of initial boundary value problems involving Maxwell's equations in isotropic media. *IEEE Trans Antennas Propag* 1966;14:302–7.
- [8] Taflov A, Hagness SC. *Computational electromagnetics*, 2nd ed. Boston, MA: Artech House; 2000.
- [9] Jackson JD. *Classical electrodynamics*. New York: Wiley; 1998.
- [10] Draine BT. The discrete-dipole approximation and its application to interstellar graphite grains. *Astrophys J* 1988;333:848–72.